Eur. Phys. J. Special Topics **227**, 73–83 (2018)

https://doi.org/10.1140/epjst/e2018-00071-3

THE EUROPEAN PHYSICAL JOURNAL SPECIAL TOPICS

Regular Article

DEM/FEM simulation for impact response of binary granular target and projectile

Shinnosuke Takeda[1,a], Kinya Ogawa[2], Kenichi Tanigaki[1], Keitaro Horikawa[1], and Hidetoshi Kobayashi[1]

[1] School of Engineering Science, Osaka University, 1-3 Machikaneyama-cho, Toyonaka, Osaka 560-8531, Japan
[2] Institute of Space Dynamics, Ondoyama, Narutaki, Ukyo-KU, Kyoto 616-8255, Japan

Received 1 August 2017 / Received in final form 10 January 2018
Published online 10 September 2018

Abstract. Three-dimensional dynamic discrete element method (DEM) and finite element method (FEM) simulation using LS-DYNA were, respectively, applied to the randomly distributed binary granular material and to the cylindrical projectiles in order to clarify the effect of size distribution of target particles on the dynamic behaviour of low density granular material. It was found that the peak resistance force of projectile during penetration depends on the packing density of the granular materials and on the impact velocity of projectile. The change of resistance force was well understood in connection with the propagation and the reflection of stress wave in projectile. The variety of particle size almost did not affect the resistance force of projectile. Densified region in granular material was generated ahead of projectile after impact. The densified region propagated in the depth direction and its propagation speed depended on the packing density of target granular material and impact velocity of projectile. That is, projectile impact behaviours of granular materials can be uniformly handled by impact velocity and packing density of the granular material, not depending on the variety of the particle size.

1 Introduction

Collision impact between continuous material and granular materials such as sand, soil, and heterogeneous brittle aggregates is one of the most interesting subject because it can be seen in many fields such as crater phenomena in the planetary science, impact pilling of concrete piles in construction of high-rise buildings, sample return device equipped on probe vehicle as Hayabusa and so on. Over several decades, therefore, a lot of experimental and analytical researches have been carried out. For example, the article titled "Dynamics of a Projectile Penetration Sand" [1] is one of early works in which a series of experiments of conical-nosed projectile penetrating randomly-packed sand and the analysis using a kind of conventional penetration formulas were involved. In 1978, a huge review with nearly 100 pages, concerning the

[a] e-mail: shinnosuke.takeda@impact.me.es.osaka-u.ac.jp

terminal ballistic aspects and the penetration mechanics was written by Backman and Goldsmith [2]. The interesting data obtained from the hyper-velocity impact [3,4] or high-speed penetration into sand [5,6] is the maximum penetration depth and/or the projectile design suitable for the deepest penetration into sand. In order to record grain and bulk response of the penetration event, various experimental techniques, i.e. high-speed photography coupled with a particle image velocimetry technique [7], buried quartz gauges for the measurement of transmitted stress wave profile, high-speed video with photo-elastic particles [8], etc. Recently, a study about the impact of a projectile onto a bed of small grains immersed in an index-matched fluid was performed to examine the effect of fluid on the impact dynamics [9]. An elegant review [10] surveyed knowledge about crater phenomena in the planetary science and penetration phenomena in granular targets.

With recent rapid development of computer, there are also many studies using numerical simulation concerning collision impact of granular materials. The discrete element method (DEM) is one of the most suitable simulation techniques capable of describing the mechanical behaviour of assemblies of discs and spheres such as sand and soil [11], because the movement of discrete particles can be treated. Wada et al. studied the impact cratering process on granular material due to vertical impact by using 3-D DEM simulations. The size of the crater cavity and the ejecta velocity were successfully compared with the results of experiments [12]. The projectile instability during penetration in dry sand was examined by 2-D DEM analysis [13]. Projectile instability was mainly caused by lateral forces due to the heterogeneous and randomness inherent in a particulate media like sand.

The effect of variations in the size distributions and variations in the dynamic fracture strength of dry sand target on the dart penetration were investigated by DEM [14]. And then, they said that both variations can have significant effect on penetration performance of the dart. By using DEM, idealized granular geometric packing subjected to gravity was studied [15]. Single-sized and multi-sized sphere packings were attempted to find the packing manner with the largest packing density by 3-D DEM code [16,17]. These topics were not a problem about impact penetration into granular target, though.

As widely used for numerical analysis of projectile impact to granular target so far, the discrete element method is quite suitable to simulate the mechanical behaviour of granular materials. However, the projectile is usually made of a continuum material. Therefore, DEM is not necessarily the best method to analyze the mechanical response of projectile. The finite element method (FEM) appears to be rather proper for this. From this consideration, the combination analysis of DEM and FEM was carried out about some dynamic geomechanics problems [18]. This combined method was successfully applied to the analysis for cutting rocks or the analysis for impact of projectile against rock plate. However, this research just proved that the combined analysis is very useful to study projectile penetration into granular target. They have not got enough results about impact problems, yet.

In this research, the goal is to investigate the dynamic mechanical responses of projectile by FEM analysis and simultaneously of granular target by DEM. The effects of packing density and impact velocity on the dynamic mechanical response of granular target were also examined.

2 Simulation

Figure 1 shows a projectile and a target of granular material used for our research. The projectile was an aluminium cylinder of 42 mm in diameter and 120 mm in length. Three-dimensional elastic FEM model was applied to the projectile having Young's modulus of 69 GPa, density of 2.8×10^3 kg/m^3 and Poisson's ratio of 0.34.

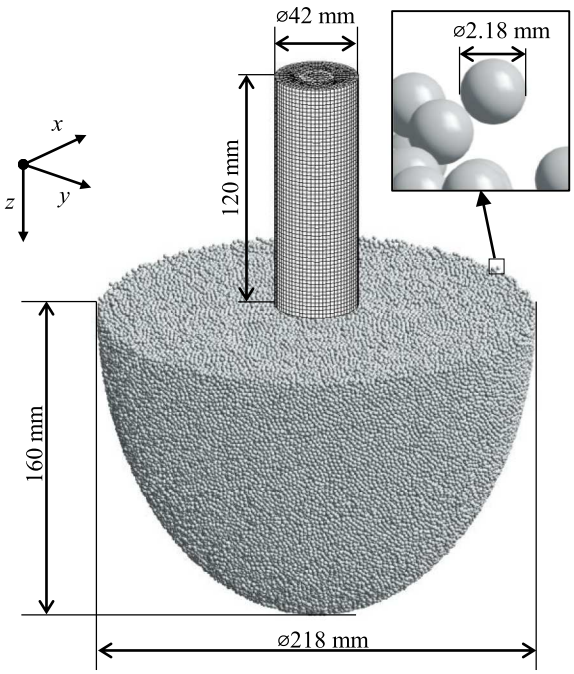

Fig. 1. Target and cylindrical projectile.

A three-dimensional rectangular coordinate *xyz*-system was set in which the z axis was reverse direction of the normal to the surface of target granular medium. The initial impact velocity, V_i was given to projectile in the range of 60–240 m/s in the z direction. Simulation was conducted under zero gravity condition.

The target granular materials consist of alumina ceramic spheres of 3.76×10^3 kg/m^3 in density with Young's modulus of 310 GPa. Movement of individual spherical particles after impact was traced by using elastic Discrete Element Method (DEM) in LS-DYNA. The particle–particle interaction was accomplished using penalty-based contact algorithms. The normal and tangential reactions were expressed by divider, spring and slider as shown in Figure 2 [11]. The divider represents that adjacent particles interact only when they contact with each other. The normal spring constant, k_{N}, and the tangential spring constant, k_{T} were as shown in table (Fig. 2).

The spring constants were computed by LS-DYNA using the material constants [19]. The slider represents frictional force based on Coulombs law of dry friction. The friction coefficient, μ and the rolling friction coefficient, μ_r were, respectively, 0.1 and 0.001. We made an original granular target which consists of randomly close packed discrete element spheres in a semi-spheroidal container of 210 mm in diameter and 160 mm in depth as shown in Figure 1. Its packing density was 63% which is a density of randomly close packed spheres [20].

By using three kinds of particles with different size (Tab. 1), particles 1, 2 and 3, we created three types of rarefied granular target materials, A, B and C. Particle 1 is the basic particle which we have used so far. The difference of particles 2 and 3 from particle 1 is only size. Particle 2 is a particle with half volume of particle 1 and particle 3 has a half diameter of particle 1 as shown in Table 1. Granular material A was generated as follows: (1) x, y and z-coordinates of the spheres in the dense original granular target which consisted of particle 1 were isotropically displaced by multiplying a desired coefficient, and (2) overflowed spheres moved across the container

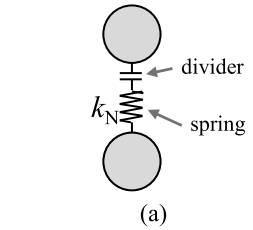

(a)

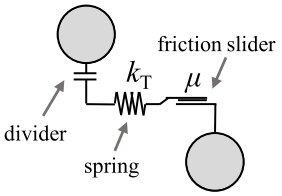

(b)

k_N [N/m]	3.13×10^9
k_T [N/m]	8.95×10^8
μ	0.1
μ_R	0.001

Fig. 2. Mechanical model of material with erastic spring and sliders to represent friction.

Table 1. Alumina ceramic particle parameters.

	Diameter [mm]	Volume [mm^3]	Material density [kg/m^3]	Young's modulus [GPa]	Poisson's ratio	Remarks
Particle 1	2.18	5.42				Basic particle
Particle 2	1.73	2.71	3.76×10^3	310	0.24	Half volume of basic particle
Particle 3	1.09	0.68				Half diameter of basic particle

were deleted. Granular materials B and C were generated as follows: (1) particles in the original dense granular target material were picked out randomly at the predetermined number of particle 2 or 3 as satisfying the desired packing density, as shown in Table 2. The picked particles were replaced by particle 2 or 3, i.e. granular material B consists of particle 1 and particle 2, and granular material C consists of particle 1 and particle 3. The packing densities chosen were ranged from about 55% to 42% as shown in Table 2. The bulk densities of the rarefied granular materials are close to those of sand and soil.

3 Simulation results and discussions

3.1 Resistance force of projectile during penetration

The resistance force during penetration of Type A granular material in the cases of various impact velocities from 60 to 240 m/s are shown in Figure 3a. The resistance forces were obtained from the axial stress of elements on the projectile head. When the

Table 2. Particle number for three types of granular materials.

Granular materials		Number of particles			
		Particle 1 (basic particle)	Particle 2 (half volume)	Particle 3 (half diameter)	Bulk density [kg/m^3]
63%	A 63%	462 300			2.37×10^3
55%	A 55%	388 262			
	B 55%	344 890	117 410		2.07×10^3
	C 55%	395 209		67 091	
50%	A 50%	352 645			
	B 50%	271 510	190 790		1.88×10^3
	C 50%	353 277		109 023	
42%	A 42%	296 247			
	B 42%	154 100	308 200		1.58×10^3
	C 42%	286 186		176 114	

projectile hit the surface of the target, the force increases rapidly with oscillation. The force was increased with the increase of impact velocity (Fig. 3a). Since the oscillation was from lateral effect of the thick projectile, hereinafter the force was smoothed with the 10 ms moving average. This significant increase of peak force, $F1$ can be understood by the change of momentum of the particles in granular material as discussed previously [21]. The force decreased periodically like a step (Fig. 3a – $F2$, $F3$) after the peak values, $F1$ appeared. The vertical dot–dash lines in Figure 3 are drawn with an interval time of 48 ms, T_r, which looks like corresponding to the step interval of force records, except for the initial part. The interval time, T_r, corresponds to the time of one return journey of elastic wave in the longitudinal direction of the projectile because of the length of 120 mm and elastic wave velocity of 5000 m/s. Therefore, the cause of this periodic change of the resistance force may be the elastic wave reflection in the projectile. Thus, we can say that the resistance force of binary granular material decreases step-by-step as same as the case of a single kind of particle granular material shown in the previous research [22].

The resistance force during penetration of Type A granular material in the cases of various initial packing densities from 63 to 42% are shown in Figure 3b. The force was increased with the increase of initial packing density (Fig. 3b).

Figure 4 shows the resistance force of single and binary granular materials with three different packing densities in the case of the same impact velocity of $V_i = 120$ m/s. Solid lines show the case of Type A granular model, composed of only one type of particle. Broken lines show the case of Type B binary granular model, composed of basic particles (particle 1) and half volume particles (particle 2). Dotted lines show the case of Type C binary granular model, composed of basic particles and particles with half diameter (particle 3). The resistance forces of three kind targets Type A, B and C differ in the oscillation. However, the peak values and the decreasing period of forces are almost same. This means that the influence of the variety of size and distribution in target particles on the resistance force is quite small and confined if the initial packing density of granular material is the same, although it is the results obtained from the limited range of packing density and distribution patterns.

3.2 Distribution of local packing density

To clarify stress wave propagation state in the granular material, we have focused our attention on the change of local packing density distribution in the depth direction in front of projectile. Figure 5a shows local packing density distribution at 300 μs

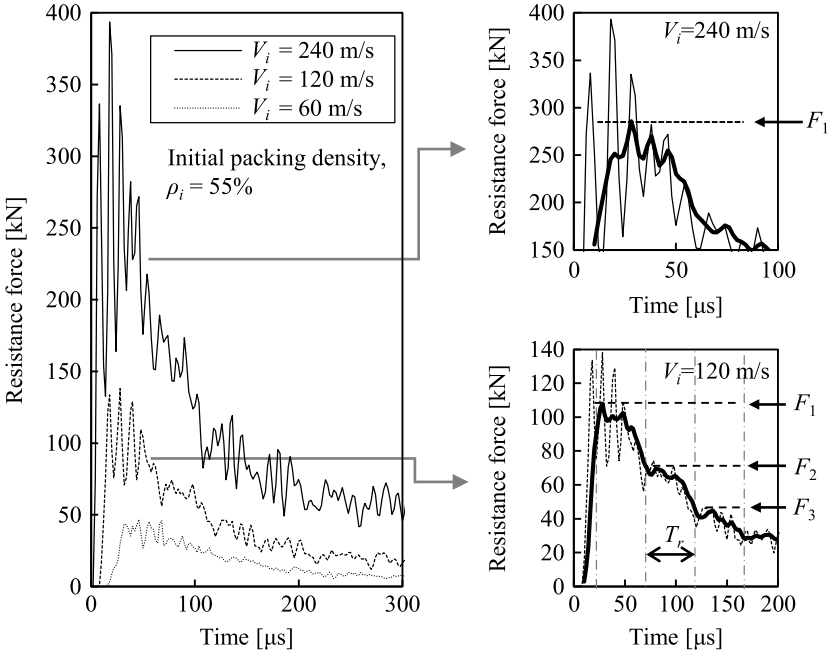

(a)

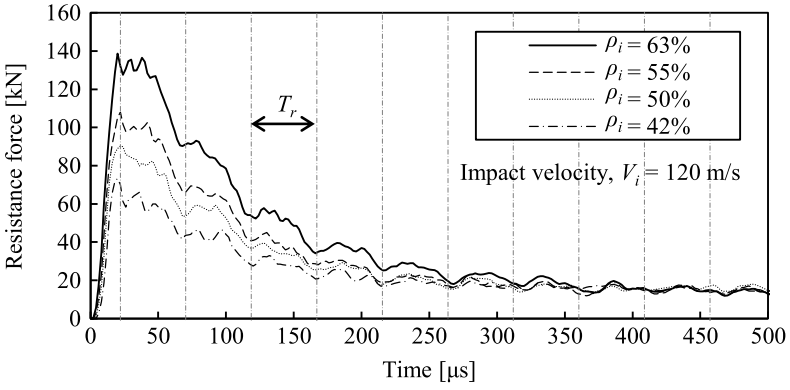

(b)

Fig. 3. Resistance force change of the granular material A. (a) Effect of impact velocity V_i on the resistance force change at initial packing density of 55%. (b) Effect of packing density on resistance force change at impact velocity of 120 m/s.

after impact in granular material with initial packing density, $\rho_i = 55\%$, for impact velocity of 120 m/s. The local packing density distribution after impact is shown by using 5 mm × 5 mm square tiles. In order to express the propagation of this dense area around the projectile head, we considered a circular cylinder with 20 mm in diameter and 150 mm in length along the z direction as shown in Figure 5a by broken line. We defined the local packing density at a depth of z mm using the range from $z - 2$ mm to $z + 2$ mm in the cylinder. The packing density may reflect to stress and strain in the sense of continuous mechanics. Figure 5b shows the local packing density distribution

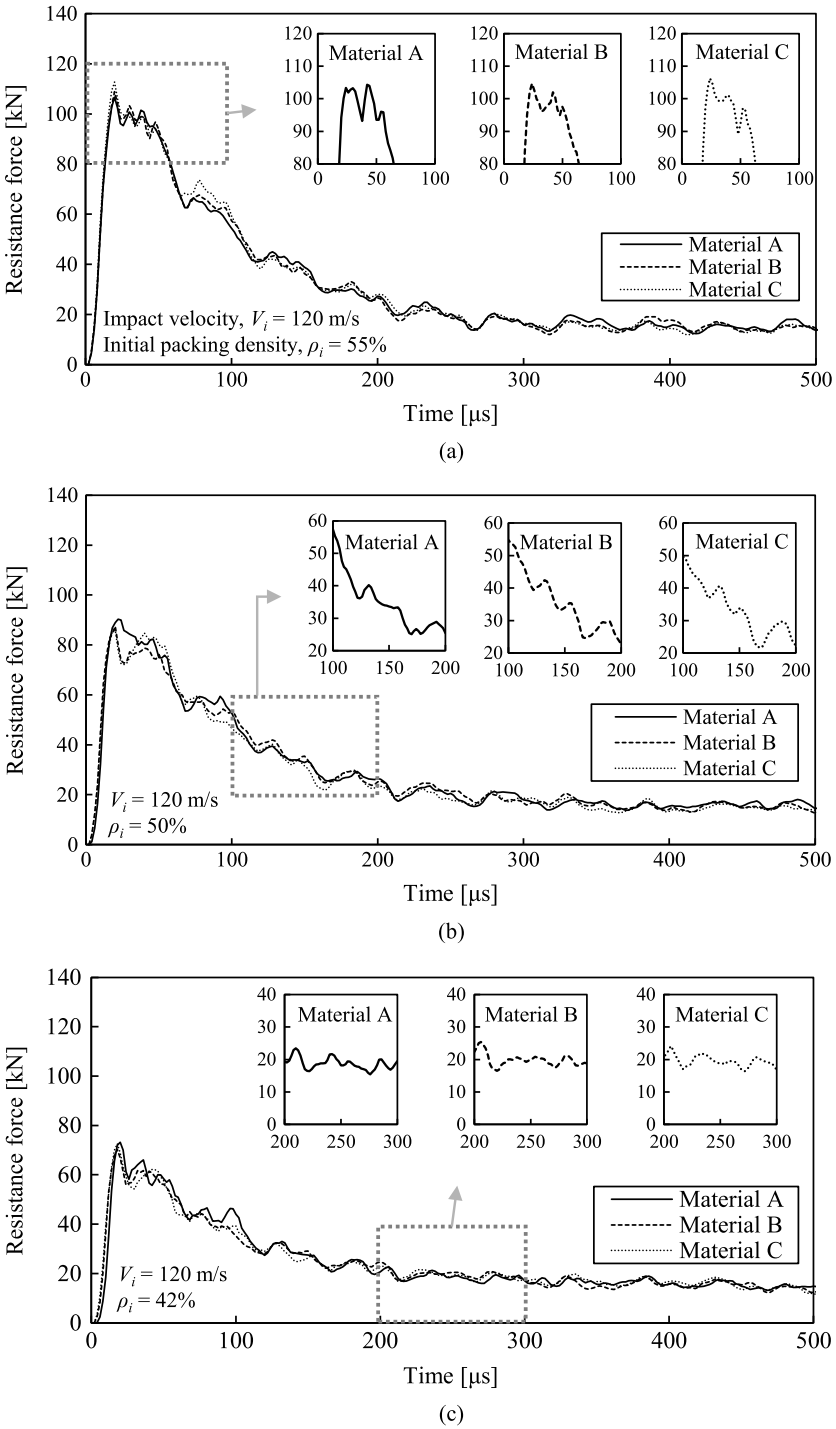

Fig. 4. Resistance force–time relations at three kinds of granular material for impact velocity, $V_i = 120\,\mathrm{m/s}$. (a) Packing density 55%. (b) Packing density 50%. (c) Packing density 42%.

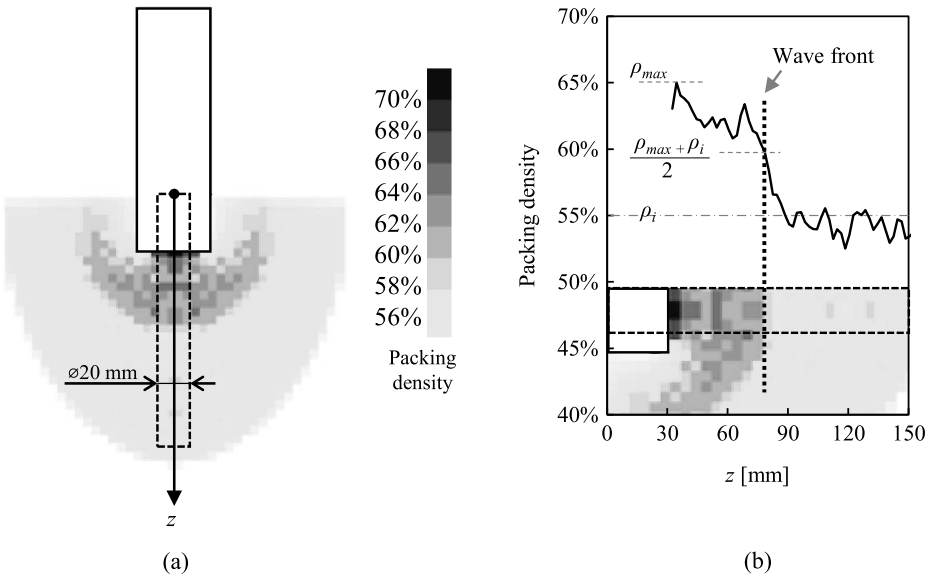

Fig. 5. Local packing density distribution in the depth direction, z at 300 μs for impact velocity 120 m/s, initial packing density 55%. (i) Surface of granular medium ($z = 0$ mm). (ii) Position of projectile head. (iii) Densified region in granular material. (iv) Wave front of propagation of densified region. (v) Bottom of granular material ($z = 150$ mm). (a) Packing density distribution in granular medium. (b) Packing density distribution in the direction of z.

in the depth, z direction at 300 μs. This figure can clearly show the dense area in front of projectile head. The depth at which the density becomes the intermediate value between the maximum density, $\rho_{\max}$ and the initial density, ρ_i is defined as the wave front.

Figure 6 shows the local packing density distributions in the depth direction for impact velocity, $V_i = 120$ m/s, respectively at 100 μs, 300 μs and 500 μs after impact. Solid lines show the granular model A, i.e. single kind particle. Broken lines show the binary granular model B. Dotted lines show model C (see Tab. 2). After impact, it can be found that the highly densified region, shown as an angulating mountain pattern, propagates in the depth direction. The propagation of densified regions in the binary granular materials were almost same as the single granular material (model A). With increase of initial packing density and impact velocity of projectile, the densified region propagated faster as with the previous study for granular medium which contains one kind of particle [21]. When we focus our attention on the magnitude of density, it is found that the magnitude of local packing density in front of projectile corresponds to the resistance force. The packing density of the densified regions at 100 μs after impact is high and it decreases gradually with time of 300 μs and 500 μs as shown in Figure 6. The similar dependency can be found in the resistance force changes presented in Figure 4. The propagation speed of the densified region in front of the projectile head depends on the initial average packing density, i.e. the propagation of densified region is faster in higher initial packing density materials than lower materials, although the packing density change seems to be independent on the variety of particle size of granular materials, because there are any significant differences among these granular material models A, B and C. The results suggest that propagation of densified region in granular materials is affected by their initial average packing density, however the influence of the variety of particle size is relatively small.

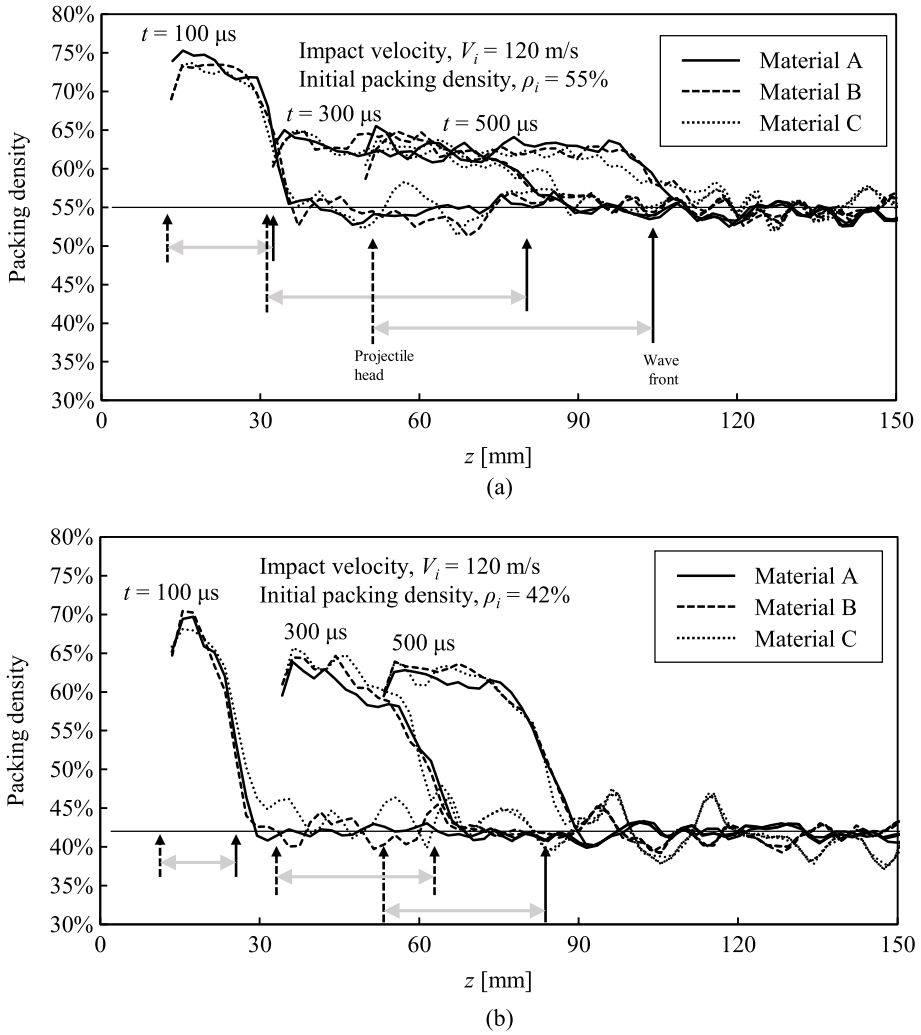

Fig. 6. Effect of initial packing density on the propagation of densified region in granular material for impact velocity of 120 m/s. (a) Initial average packing density of 42%. (b) Initial average packing density of 55%.

When the force applied to the projectile from a granular target and the time increment are, respectively, denoted to be F and dt, the impulse can be expressed by the change of momentum as follows:

$$F\mathrm{d}t = \rho AC\mathrm{d}tV, \tag{1}$$

where ρ, A and C are, respectively, the density of densified region, a hypothetical cross-sectional area and the propagation speed of the densified region in front of the projectile head. Since $\rho AC\mathrm{d}t$ corresponds to the mass of granular target accelerated to be a velocity V. While, the force applied to the head of projectile can be written by $F = \sigma A_0$, where σ and A_0 are the mean stress and the cross-sectional area of the

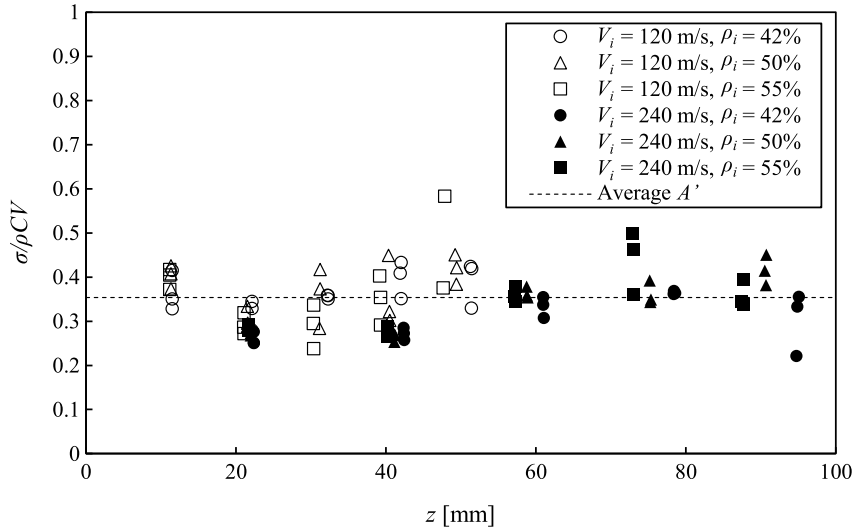

Fig. 7. Evaluated value of A' during penetration.

projectile. Therefore, equation (1) can be rewritten as follows:

$$\sigma A_0 = \rho ACV \quad \Rightarrow \quad \sigma = \rho A' CV, \quad A' = \frac{A}{A_0}, \tag{2}$$

where A' is a cross-sectional areas ratio of A to A_0.

Figure 7 shows A' $(=\sigma/\rho CV)$ during penetration for the various impact velocities $(V = 60 - 240\,\mathrm{m/s})$ and initial packing densities $(\rho_0 = 42 - 63\%)$. The ρ is given by the value of $\rho_{\max}$ in Figure 5 and/or Figure 6. The C can be evaluated from the propagation velocity of the densified region front in a target material obtained from Figure 5 and/or 6 with a 100 μs interval, while V may be obtained from the change of the projectile head location in Figure 5 and/or 6 with a 100 μs interval. The values of A' are almost constant and less than one. The reason may be explained by taking account that not all particles are moving at the same velocity, V as that of projectile. Thus, the cross-sectional area ratio corresponding to the velocity distribution ratio is independent on the initial target density and the impact velocity.

4 Concluding remarks

Three-dimensional dynamic FEM and DEM simulations for the projectile penetration into granular target material were carried out to investigate the effect of the size variety in granular particle on the dynamic behaviour of projectile and granular target. The major results obtained are: (1) the resistance force of projectiles during penetrating single or binary granular material depends on the initial packing density of granular target materials and on the impact velocity. (2) The propagation velocity of highly densified region in granular target material increased with the increase of the initial packing density and with the increase of impact velocity and is not affected by the variety of particle size in granular target. (3) The ratio of the hypothetical cross-sectional area of the densified region in front of the projectile head to the cross-sectional area of projectile is about 0.35 during penetration, which is almost constant

even the impact velocity or the initial packing density of granular target materials changes.

Author contribution statement

Shinnosuke Takeda contributed to the design and implementation of the research, to the analysis of the results and to the writing of the manuscript with support from Kinya Ogawa, Kenichi Tanigaki, Keitaro Horikawa and Hidetoshi Kobayashi. Hidetoshi Kobayashi and Kinya Ogawa supervised the project.

References

1. W.A. Allen, E.B. Mayfield, H.L. Morrison, J. Appl. Phys. **28**, 370 (1957)
2. M.E. Backman, W. Goldsmith, Int. J. Eng. Sci. **16**, 1 (1978)
3. A.F. Savvateev, A.V. Budin, V.A. Kolikov, P.G. Rutberg, Int. J. Impact Eng. **26**, 1 (2001)
4. B. Hermalyn, P.H. Schultz, Icarus **216**, 269 (2011)
5. V.G. Bazhenov, A.M. Bragov, V.L. Kotov, J. Appl. Mech. Tech. Phys. **50**, 1011 (2009)
6. A. Van Vooren, J. Borg, H. Sandusky, J. Felts, Procedia Eng. **58**, 601 (2013)
7. J.P. Borg, M.P. Morrissey, C.A. Perich, T.J. Vogler, L.C. Chhabildas, Int. J. Impact Eng. **51**, 23 (2013)
8. A.H. Clark, A.J. Petersen, L. Kondic, R.P. Behringer, Phys. Rev. Lett. **114**, 1 (2015)
9. K.N. Nordstrom, E. Lim, M. Harrington, W. Losert, Phys. Rev. Lett. **112**, 1 (2014)
10. J.C. Ruiz-Suárez, Rep. Prog. Phys. **76**, 66601 (2013)
11. P.A. Cundall, O.D.L. Strack, Géotechnique **29**, 47 (1979)
12. K. Wada, H. Senshu, T. Matsui, Icarus **180**, 528 (2006)
13. S.K. Dwivedi, R.D. Teeter, C.W. Felice, Y.M. Gupta, J. Appl. Phys. **104**, 83502 (2008)
14. J.P. Borg, T.J. Vogler, Int. J. Impact Eng. **35**, 1435 (2008)
15. M.A. Faraone, J.H. Chung, M.T. Davidson, Discrete element analysis of idealized granular geometric packings subjected to gravity, in *10th European LS-DYNA Conference 2015, Würzburg, Germany* (2015)
16. Z. Han, H. Teng, J. Wang, Computer generation of sphere packing for discrete element analysis in LS-DYNA, in *12th International LS-DYNA® Users Conference* (2012), pp. 1–4
17. S. Yamada, J. Kanno, M. Miyauchi, Inf. Media Technol. **6**, 493 (2011)
18. E. Oñate, J. Rojek, Comput. Methods Appl. Mech. Eng. **193**, 3087 (2004)
19. N. Karajan, Z. Han, H. Teng, J. Wang, Interaction possibilities of bonded and loose particles in LS-DYNA, in *9th European LS-DYNA Conference* (2013), pp. 1–27
20. G.D. Scott, D.M. Kilgour, J. Phys. D.: Appl. Phys. **2**, 863 (1969)
21. K. Ogawa, S. Takeda, H. Kobayashi, Mech. Eng. J. **2**, 14 (2015)
22. K. Ogawa, S. Takeda, H. Kobayashi, K. Tanigaki, EPJ Web Conf. **94**, 4040 (2015)